Clothing and Carrying Condition Invariant Gait Recognition based on Rotation Forest

Sruti Das Choudhury, Tardi Tjahjadi

School of Engineering, University of Warwick Gibbet Hill Road, Coventry, CV4 7AL, United Kingdom.

Abstract

This paper proposes a gait recognition method which is invariant to maximum number of challenging factors of gait recognition mainly unpredictable variation in clothing and carrying conditions. The method introduces an averaged gait key-phase image (AGKI) which is computed by averaging each of the five key-phases of the gait periods of a gait sequence. It analyses the AGKIs using high-pass and low-pass Gaussian filters, each at three cut-off frequencies to achieve robustness against unpredictable variation in clothing and carrying conditions in addition to other covariate factors, e.g., walking speed, segmentation noise, shadows under feet and change in hair style and ground surface. The optimal cut-off frequencies of the Gaussian filters are determined based on an analysis of the focus values of filtered human subject's silhouettes. The method applies rotation forest ensemble learning recognition to enhance both individual accuracy and diversity within the ensemble for improved identification rate. Extensive experiments on public datasets demonstrate the efficacy of the proposed method.

Keywords: Gait averaged gait key-phase image, Gaussian filter, focus value, rotation forest ensemble classifier.

1. Introduction

Gait recognition plays a significant role in visual surveillance as it enables human identification at a distance using low resolution video sequences. However, variation in view, clothing and carried items bring main challenges to any shape-analysis based gait recognition method, as these factors considerably distort the shape of a silhouette. Human identification based on gait is also adversely affected by variation in walking speed, shadows under feet, and presence of occluding objects.

Gaussian filter is a band-pass filter, i.e., a combination of lowpass Gaussian filter (Lp-Gf) and a highpass Gaussian filter (Hp-Gf) [8]. This paper introduces a gait recognition method based on filtering which involves a Lp-Gf and a Hp-Gf at different cut-off frequencies to achieve invariance to unpredictable variation in clothing and carrying conditions in addition to other covariate factors, namely, variation in walking speed, segmentation noise, missing and distorted frames, change in ground surface and hair style, shadows under feet and occlusions. Lp-Gf causes smoothing or blurring of a silhouette and thus reduces noise. As the cut-off frequency of the Lp-Gf decreases, there is a gradual loss of boundary and exterior region. Thus, the application of Lp-Gf with decreasing cut-off frequencies gradually highlights the characteristics of inner part of a silhouette towards its central region more than its boundary, enabling the proposed method to achieve robustness against tight versus loose clothing, and clothing type variation. It also reduces the effect of shape distortions at the silhouette boundary due to small carried items. The use of Hp-Gf at

the same cut-off frequencies retains the boundary and the exterior parts of a silhouette more than the central part, thus highlighting the boundary characteristics of the silhouettes. Thus, it enables improved inter-subject discrimination in the absence of change in covariate factors. The cut-off frequencies of the Gaussian filters for optimal performance are determined experimentally based on an analysis of the focus values of the silhouettes.

Several state-of-the-art gait recognition methods [4, 27, 3] analyse the dynamic and/or static gait characteristics of silhouettes or the extreme outer boundary of silhouettes, i.e., contours of a gait sequence for identifying a human subject. The performance of these methods largely depends on the correctness of the background segmentation techniques, presence of occluding objects in the scene and shadows under feet, as these factors considerably determine the quality of the silhouettes and the extracted contours. In addition, analysing all the silhouettes of a gait sequence individually, increases computation time and requires more storage space. [11] thus introduced a novel concept of gait energy image (GEI) which is formed by averaging all the silhouettes of a gait period to capture spatio-temporal gait characteristics in a single image to facilitate noise-resilient gait feature extraction in reduced space and time complexity. However, since GEI averages all the silhouettes of a gait period, it does not preserve the important distinctive gait characteristics of different phases of a gait period. To overcome this limitation, this paper introduces an averaged gait key-phase image (AGKI) by averaging key-phases of the gait periods over a gait sequence.

It has been experimentally shown in [12] that the random subspace method outperforms other ensemble classification methods, e.g., bootstrapping [2] and Adaboost [6], in the case of high dimensionality of the feature space for a small number of gallery samples. The gait recognition method in [10] demonstrated that random subspace ensemble classifier method provides improved gait recognition rate by effectively avoiding overfitting due to high dimensionality of the feature space compared to the available number of gallery samples, which are often recorded at a particular walking condition. Random subspace method combines the identification rates of the component classifiers associated with the randomly selected independent feature subsets of dimensions smaller than the original feature space using majority voting policy, and significantly outperforms single classifiers, e.g., nearest neighbour (NN), support vector machine and Bayesian classifier in gait recognition.

Relying on the basic principle of random subspace method, the main motivation of introducing the rotation forest ensemble classifier in [21] is to simultaneously encourage member diversities and individual accuracy within a classifier ensemble. Although the superiority of random forest over bagging and AdaBoost has been demonstrated on 33 datasets from the UCL repository in [21] and three widely used datasets, i.e., NASAs Airborne Visible Infra-Red Imaging Spectrometer, Reflective Optics System Spectrographic Imaging System, and Digital Airborne Imaging Spectrometer for hyperspectral image classification in [28], its efficacy has yet to be explored in gait recognition. Thus, the paper introduces the use of rotation forest ensemble classifier in gait recognition, and experimentally demonstrates its superiority to random subspace method in this field by simultaneously encouraging

individual accuracy and diversity within the ensemble in addition to overfitting avoidance.

The rest of the paper is organized as follows. Section 2 discusses related works and Section 3 presents the proposed method. Section 4 presents the experimental results, and Section 5 concludes the paper.

2. Related work

Various markerless gait recognition methods (model-based and model-free) have been proposed in the literature to address one or more covariate factors of gait. Model-based methods (e.g., [17, 23, 9]) use a structural model to measure time-varying gait parameters, e.g., gait period, stance width and stride length, and a motion model to analyse the kinematical and dynamical motion parameters of the subject, e.g., rotation patterns of hip and thigh, and joint angle trajectories, to obtain gait signatures. The model-free gait recognition methods in [4, 3, 27] analyse the dynamic and/or static gait characteristics of silhouettes or the extreme outer boundary of silhouettes, i.e., contours of a gait sequence. The performance of these methods largely depends on the correctness of the background segmentation techniques, presence of occluding objects in the scene and shadows under feet, as these factors considerably determine the quality of the silhouettes and the extracted contours. In addition, analysing all the silhouettes of a gait sequence individually, increases computation time and requires more storage space. Hence, the introduction of GEI [11]. Since then many promising model-free gait recognition methods have been proposed based on a GEI,e.g., [26, 15, 29, 24, 1, 5] to outperform the original method of GEI.

The boundary shape distortions due to variation in clothing of the same subject decrease the identification rate. Therefore, the method in [13] applies part-based strategy to adaptively assign more weight to body parts that remain unaffected due to clothing variation and less weight to affected body parts based on a probabilistic framework. However, it is unrealistic to train the model with all known clothing types in realistic scenario. The method in [14] assigns depth information to binary silhouettes using 3-dimensional (3D) radial silhouette distribution transform and 3D geodesic silhouette distribution transform. The gait features extracted by radial integration transform, circular integration transform and weighted Krawtchouk moments are fused using a genetic algorithm (RCK-G). RCK-G is robust to limited clothing variation, but sensitive to carrying conditions.

The methods in [3, 4, 20] aim to achieve invariance to carrying conditions. The method based on spatio-temporal motion characteristics, statistical and physical parameters (STM-SPP) [3] analyses the shape of a contour using Procrustes analysis at the double support phase and elliptic Fourier descriptors (EFDs) at ten phases of a gait period. The method in [4] combines model-based and model-free approaches to analyse the spatio-temporal shape and dynamic motion (STS-DM) characteristics of a subject's contour. A part-based EFD analysis and a component-based FD analysis based on anthropometry are respectively used in STM-SPP and STS-DM to achieve robustness to small carried items. The method in [20] uses an iterative local curve embedding algorithm

to extract double helical signatures from the subject's limb to address shape distortion due to a specific carrying condition, e.g., a briefcase in upright position.

While existing gait recognition methods have only considered the predefined and limited variation in clothing and carrying conditions, the proposed method achieves robustness against unpredictable variation in clothing and carrying conditions as well as several other covariate factors.

3. Proposed method

3.1. Module 1: Feature extraction

3.1.1. AGKI formation

The normalised and centre-aligned silhouettes provided by the publicly available datasets are used as the input gait sequences of the proposed method for feature extraction. A gait period starts with the heel strike of either foot and ends with the subsequent heel strike of the same foot and comprises two steps. Each foot in a gait period transits between two phases: a stance phase when the foot remains in contact with the ground and a swing phase when the foot does not touch the ground. The components of stance phase are: initial contact, mid-stance and propulsion. The components of swing phase are: pre-swing, mid-swing and terminal swing. A detailed description of these phases are provided in [3].

The gait periods are determined from the video sequence of lateral view of the subject by the number of frames between two frames of a gait sequence with the most foreground pixels enclosed in the region bounded by bottom of the bounding rectangle and the anatomical position of just before the subject's hand measured from the bottom (i.e., 0.377H where H is height of the bounding rectangle) because this foreground region, i.e., the bottom segment of the bounding rectangle is not distorted by self-occlusions due to arm-swing (see Fig.3 of [4]). After estimating the gait period, its five key-frames (i.e., double support, midstance, midswing, ending swing and propulsion) which capture most of the significant gait characteristics, are extracted using region-of-interest based contour matching based on weighted Krawtchouk moments following the procedure in [4].

The Krawtchouk moments of order $(n+m)$ of a $N \times M$ silhouette with intensity function $f(x,y)$ are computed using the sets of weighted Krawtchouk polynomials $\overline{K}_n(x; p, N)$ and $\overline{K}_m(x; p, M)$ as [14]

$$Q_{nm} = \sum_{x=0}^{N-1} \sum_{y=0}^{M-1} \overline{K}_n(x; p1, N-1).\overline{K}_m(y; p2, M-1).f(x,y), \tag{1}$$

where $n = 0, 1, ..., N$ and $m = 0, 1, 2, ..., M$. The set of weighted Krawtchouk polynomials, i.e., $\overline{K}_n(x; p, N)$ is defined as

$$\bar{K_n}(x; p, N) = K_n(x; p, N) \sqrt{\frac{w(x; p, N)}{\rho(n; p, N)}}, \text{where} \quad p \in (0, 1), \tag{2}$$

and

$$\rho(n; p, N) = (-1)^n \left(\frac{1-p}{p}\right)^n \frac{n!}{(-N)_n}. \tag{3}$$

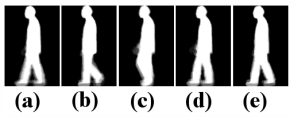

Fig. 1. AGKIs for different phases of gait period: (a) double support; (b) midstance; (c) midswing; (d) ending swing; and (e) propulsion.

The five key-frames of a gait period are manually extracted from OU-ISIR gait dataset and the bottom segment of the bounding rectangles of these key-frames are set as the reference Region-of-Interests (Rf-ROIs). The same silhouette segments of all frames of a subject's gait period are each referred to as a target Region-of-Interest (Tr-ROI). The proposed method computes weighted Krawtchouk moments of each of the Rf-ROIs and Tr-ROIs using Eq.(1) by suitably choosing the values of N (say, c) and M (say d) (such that they respectively denote the width and height of the bottom segment of the bounding rectangle) of order (c + d) using p = 0.5. Gait sequence consists of many gait periods. Each of the key-phases thus obtained from all the gait periods of a gait sequence are individually averaged to form AGKI. Thus, five AGKIs corresponding to five key-phases are obtained from a gait sequence as shown in Fig. 1. Note that GEI averages all the frames of a gait period, and thus, does not consider the distinct gait characteristics at different phases of a gait period.

To automatically obtain the five key-frames of a gait period, the Rf-ROIs are compared with the target Region-of-Interest (Tr-ROI) using silhouette comparison based on weighted Krawtchouk moments to obtain similarity scores [7, 4] $S_{score} = \left[(\text{Rf-ROI}_{k_{nm}} - \text{Tr-ROI}_{k_{nm}}\right.$ where $\text{Rf-ROI}_{k_{nm}}$ and $\text{Tr-ROI}_{k_{nm}}$ respectively denote the $(c+d)$ order weighted Krawtchouk moments of the Rf-ROI and Tr-ROI. The frame whose Tr-ROI results in the lowest S_{score} with the corresponding Rf-ROI is extracted as one of the five key-frames, and the process continues by comparing the next Rf-ROI with the remaining Tr-ROIs until all five key-frames are obtained.

Since the shape characteristics of the key-frames, namely, double support, midswing and ending swing are highly distinct from each other (see Fig. 1), they are extracted very precisely from the gait sequences of the USF and OU-ISIR gait datasets. However, there are some cases where the double support and propulsion phases are extracted interchangeably due to less differences between them especially for the USF dataset, as the silhouettes of this dataset are noisy due to the presence of disjoint holes in the body and shadows under feet. Also, the performance of gait period detection from a gait sequence depends on the precise estimation of the bottom segment of the bounding rectangle. Based on the pixel count, a gait period might be overestimated, i.e., containing more images after ending swing, or underestimated. If the gait period is overestimated, the five key-frames are obtained perfectly, otherwise the nearest match is obtained if the exact match is not found. Since, the AGKIs are formed by averaging the key-frames over a gait sequence, the few erroneously extracted key-frames are not significantly manifested in the AGKIs.

3.1.2. Gaussian filtering

Spatial domain filtering is computationally faster than the frequency domain filtering for small value of standard deviation (kernel size), but its computational complexity increases as the size of the filter kernel increases. Whereas, the computational

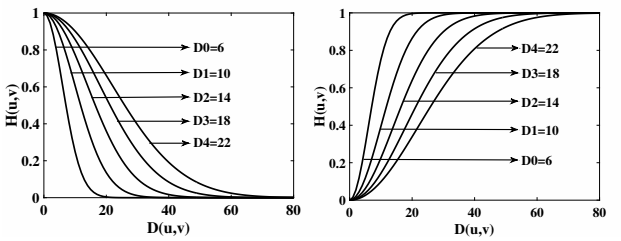

(a) (b)

Fig. 2. Radial cross-section of (a) Lp-Gf and (b) Hp-Gf for different values of cut-off frequency.

complexity of the frequency domain filtering is independent of the kernel size. More importantly, the proposed method uses different cut-off frequencies for Lp-gf and Hp-Gf, thus frequency domain filtering is preferred. Fig. 2(a) and (b) respectively show the radial cross-sections of the Lp-Gf and Hp-Gf at different cut-off frequencies used in the method. The proposed method analyses AGKIs using Lp-Gf and Hp-Gf in frequency domain at different cut-off frequencies. The Discrete Fourier Transform (DFT) of an $M \times N$ AGKI $I(x, y)$ is computed. The Fourier transformed AGKI, i.e., $DFT(u, v)$ is translation invariant, but since it exhibits the translational property of DFT, it is subjected to shift operation to ensure that the zero-frequency components are at the centre. To represent the inner part of a silhouette gradually towards the centre more than its boundary, Lp-Gf is applied to the Fourier transformed image using selected cut-off frequencies, i.e.,

$$DFT_L(u, v) = DFT(u, v)e^{(-(u^2+v^2)/2D^2)}, \tag{4}$$

where $e^{(-(u^2+v^2)/2D^2)}$ is the transfer function of Lp-Gf [8], and $DFT_L(u, v)$ denotes the image filtered using Lp-Gf at the cut-off frequency D. The filtered AGKI at cut-off frequency D in the image space is obtained by applying inverse DFT. Fig. 3(a)-(k) show the AGKIs filtered by Lp-Gf with decreasing cut-off frequency, and Fig. 3(w)-(ag) show the corresponding Fourier spectrum. Since Lp-Gf attenuates high frequency components, it blurs the AGKI and smooths detailed clothing curvatures at its boundary. As the cut-off frequency decreases, it results in a greater loss of boundary and exterior regions (due to increase in blurring) to gradually highlight the inner shape characteristics. Gaussian functions in the spatial and frequency domain behave reciprocally, hence an increase in standard deviation of Lp-Gf in the spatial domain results in more blurring and vice versa [8].

To represent the boundary and exterior regions of an AGKI more than its central part, Hp-Gf is applied to the AGKI at the same cut-off frequencies, i.e.,

$$DFT_H(u, v) = DFT(u, v)(1 - e^{(-(u^2+v^2)/2D^2)}), \tag{5}$$

where $1 - e^{(-(u^2+v^2)/2D^2)}$ is the transfer function of Hp-Gf with cut-off frequency D [8]. The filtered AGKI is similarly obtained using inverse DFT. Fig. 3(l)-(v) shows the AGKIs filtered by Hp-Gf with decreasing cut-off frequency and Fig. 3(ah)-(ar) show the corresponding Fourier spectrum. Hp-Gf emphasizes the high frequency components but retains limited low frequency components,

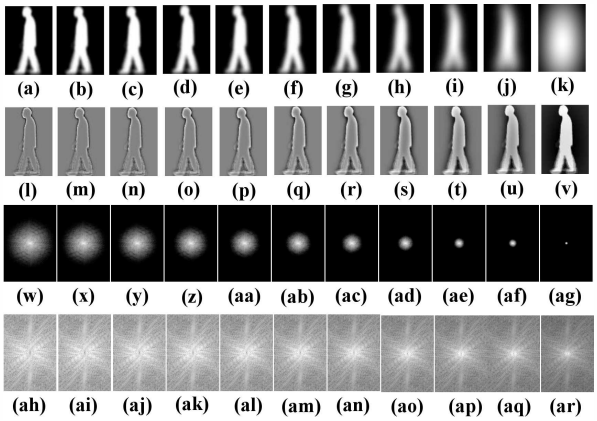

Fig. 3. Application of Lp-Gf (Row 1) and Hp-Gf (Row 2) to a AGKI from OU-ISIR dataset with decreasing cut-off frequency: (a) & (l) D_1 = 20; (b) & (m) D_2 = 18; (c) & (n) D_3 = 16; (d) & (o) D_4 = 14; (e) & (p) D_5 = 12; (f) & (q) D_6 = 10; (g) & (r) D_7 = 8; (h) & (s) D_8 = 6; (i) & (t) D_9 = 4; (j) & (u) D_{10} = 3; and (k) & (v) D_{11} = 1. Fourier spectrum at the corresponding cut-off frequencies; row 3 (Lp-Gf) and row 4 (Hp-Gf).

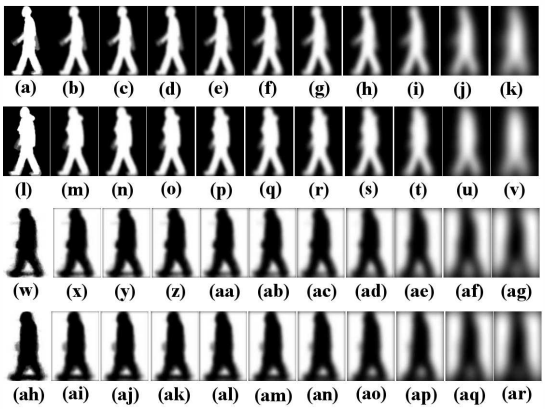

Fig. 4. (a) The original AGKI wearing (a) standard clothes and (l) down jacket from OU-ISIR gait dataset. The original AGKI (w) walking on grass without a briefcase and (ah) walking on concrete with a briefcase from USF gait dataset. Application of Lp-Gf at at the cut-off frequencies D_1 = 20, D_2 = 18, D_3 = 16, D_4 = 14, D_5 = 12, D_6 = 10, D_7 = 8, D_8 = 6, D_9 = 4, D_{10} = 3 on the AGKIs from OU-ISIR gait dataset (row 1 and 2) and USF gait dataset (row 3 and 4).

thus making the boundary characteristics of a silhouette more prominent, and its application represents the exterior regions of a AGKI as the cut-off frequency decreases. We used separable kernel to reduce the computational complexity of applying Gaussian filters to an image of height h and width w to O($w_k wh$)+O($h_k wh$) as opposed to O($w_k w_h wh$) for a non-separable kernel, where w_k and w_h respectively denote the width and height of the kernel.

Fig. 4 demonstrates the robustness of the proposed method against variation in view and surface, and the presence of a carried item with examples from two gait datasets, i.e., OU-ISIR gait dataset and USF HumanID gait dataset. Fig. 4(a)-(k) and (l)-(v) respectively show the AGKI of a subject wearing standard clothes (type 9) (gallery) and the same subject with down jacket (probe) from OU-ISIR gait dataset with their filtered versions using Lp-Gf at the cut-off frequencies D_1 = 20, D_2 = 18, D_1 = 16, D_1 = 14, D_1 = 12, D_1 = 10, D_1 = 8, D_1 = 6, D_1 = 4, D_1 = 3. Similarly, Fig. 4(w)-(ag) and (ah)-(ar) respectively show the AGKIs of a subject walking on grass without a briefcase (gallery) and the same subject carrying a briefcase walking on a concrete surface (probe) from the USF dataset with their filtered versions using Lp-Gf at the same cut-off frequencies. It is evident from Fig.3(l) and Fig.3(ah)

when respectively compared to Fig.3(a) and Fig.3(w), that the variation in clothing, carrying and surface cause significant shape alterations at the boundary resulting in high intra-subject discrimination. The alteration decreases as the blurriness increases, and disappears in the last column, where there is no difference between the gallery and its corresponding probe subject.

3.1.3. Cut-off frequency selection

The cut-off frequencies for Hp-Gf and Lp-Gf are selected based on focus value analysis of silhouettes. The focus value used to measure the degree of sharpness of an image, is the maximum for the most focused, i.e., the original silhouette. It is inversely proportional to the image blurriness caused by the Gaussian filtering at different cut-off frequencies. It has been graphically demonstrated in [30] that the wavelet based method of computing focus value has the sharpest focus measure profile and higher depth resolution compared to the spatial domain based methods, e.g., Tenengrad [25] and sum modified Laplacian [19], due to the localised support property of wavelet basis. The first level 2D Daubechies-6 wavelet decomposition of a silhouette image $f(x, y)$ of size $M \times N$ results in four subband images, W_{LL}, W_{HL}, W_{LH} and W_{HH}, where L and H respectively denote lowpass filtered and highpass filtered, and their order denotes the order of the filtering applied, e.g., W_{HL} is a subband image obtained by highpass filtering followed by lowpass filtering. The focus value (FV) of a silhouette is measured using [30]

$$FV = \frac{1}{MN} \sum_{y=0}^{N} \sum_{x=0}^{M} (|W_{HL}(x, y)| + |W_{LH}(x, y)| + |W_{HH}(x, y)|). \tag{6}$$

The focus value of the original silhouette always reduces to below 50% if it is filtered by Lp-Gf at cut-off frequency $D = 20$, and decreases linearly as the blurriness increases with decreasing cut-off frequencies. If the cut-off frequency is decreased further to below $D = 8$, the focus value decreases abruptly. The focus value becomes infinitesimally small if $D < 4$, resulting in excessively blurred silhouette without any discriminating information (e.g., Fig. 3(j)-(k)). The boundary of a silhouette is obtained by the application of Hp-Gf using D approximately in the range [18,22] for the USF dataset [22]. Since the silhouette boundary corresponds to the sharpest image, e.g., Fig. 3(l)-(m), the focus value of a silhouette filtered by Hp-Gf using D in this range remains the maximum which is considerably higher than the focus value of the original silhouette (i.e., Fig. 5(b)). With further decrease in cut-off frequency, the focus value decreases linearly with a decrease in sharpness of the image as the silhouette is reconstructed by regaining its central region. The focus value is nearly identical to that of the focus value of the original silhouette in the range $1 \leq D < 4$ due to almost perfect reconstruction of the original silhouette. Since the boundary as well as central shape characteristics of a silhouette are considered separately by using Lp-Gf and Hp-Gf, it is not necessary to use cut-off frequencies in the range $1 \leq D < 4$ which will increase the computational complexity. Thus, [4,20] is considered to be the ideal range of cut-off frequencies.

Fig. 5 (a) and (b) respectively show the normalised focus value w.r.t. decreasing cut-off frequencies in the range [22,0] of a silhouette filtered by Lp-Gf and Hp-Gf, where normalised focus values are obtained by dividing the focus values with the maximum

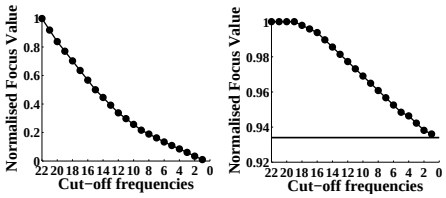

(a) (b)

Fig. 5. Normalised focus value w.r.t. decreasing cut-off frequencies of a silhouette from USF 2.1 dataset filtered using (a) Lp-Gf; and (b) Hp-Gf. '-' denotes focus value of the original silhouette.

focus value in the range [22,0]. Fig. 5 shows the focus value of a filtered silhouette maintains an almost linear relationship with the cut-off frequencies of the Gaussian filters.

The identification rate of a gait recognition method increases if the discriminability between the different subjects is high, while the same subject shows similar shape characteristics despite variation in clothing and carrying conditions in different situations. Also, the computational complexity is directly proportional to the the number of cut-off frequencies. Hence, we chose the minimum three cut-off frequencies based on the following three cases. For case 1, the discriminability between different subjects with no variation in clothing and carrying conditions is high: least blurring (for Lp-Gf) and accurate boundary (for Hp-Gf) are desirable to satisfy this. Thus, the upper cut-off of the ideal range of cut-off frequencies, i.e., D=20 for both Lp-Gf and Hp-Gf is selected. For case 2, i.e., same subjects with small shape distortions due to variation in carrying conditions, hair style and presence of shadows under feet show similar shape characteristics: medium blurring and considerably regained central region of the AGKI are desirable. Hence, the mid value of the ideal range of cut-off frequency, (i.e., D=12) for lp-Gf and lower cut-off frequency for Hp-Gf, (i.e., D=4) are chosen. For case 3, the drastic shape variation of the same subject due to unpredictable variation in clothing is taken into account. Thus, the cut-off frequency which causes excessive blurring for Lp-Gf, i.e., the lower bound of the ideal range of cut-off frequencies, i.e, D=4 is chosen. For Hp-Gf, this requires midway of the prominent boundary and almost reconstruction of the original silhouette, hence, D = 12 is appropriate. Thus, the three cut-off frequencies chosen for Lp-Gf and Hp-Gf are 4, 12 and 20. In view of this experimental analysis, the following inferences are made for any dataset:

- 1: The cut-off frequency for Lp-Gf at which the focus value of the original silhouette always reduces to below 50% can be used for Hp-Gf to obtain the boundary of the silhouette. This frequency is chosen as the upper-bound of the ideal range of the cut-off frequencies.

- 2: The cut-off frequency for Lp-Gf below which the focus value becomes infinitesimally small can be used as the cut-off frequency for Hp-Gf at which the silhouette is perfectly reconstructed. This frequency is chosen as the lower-bound of the ideal range of cut-off frequencies.

- 3: For clothing and carrying condition invariance in low computational complexity, the upper-bound, lower-bound and their

mid-value are used.

3.2. Module 2: subject classification using rotation forest

3.2.1. Training

Let $\mathbf{x} = [\mathbf{x_1}, ..., \mathbf{x_n}]^\mathbf{T}$ be a gallery subject described by n features, where n=30 corresponds to the five AGKIs filtered using Lp-Gf and Hp-Gf, each at 3 cut-off frequencies (i.e., $5 \times 3+3=30$), and N be the total number of subjects in the gallery. The gallery dataset, i.e., $\mathbf{X}$, is thus represented by $N \times n$ matrix. Let $\mathbf{Y} = [\mathbf{y_1}, ..., \mathbf{y_N}]^\mathbf{T}$ be the class labels {1,...,c} for the dataset, and c be the total number of gallery classes of subjects. Let D_1, ..., D_L denote the classifiers in the ensemble, and $\mathbf{F}$, the feature set. The steps to train the classifier D_i for i=1,...,L are:

- F is randomly split into K disjoint subsets, and each subset contains $M=n/K$ features.
- Let $F_{i,j}$ be the jth subset of features for D_i containing $X_{i,j}$ features from X, where j=1,...,K. A new training set, i.e., $X'_{i,j}$, is selected from $X_{i,j}$ randomly with 75% size using bootstrap algorithim. $X'_{i,j}$ is subjected to principal component analysis (PCA) to obtain the principal components, i.e., $a_{i,j}^{(1)}$,..., $a_{i,j}^{(M_j)}$ each of size $M \times 1$. PCA is used as the transformation algorithm due to its superiority to independent component analysis, maximum noise fraction and local Fisher discriminant analysis for the case of rotation forest ensemble classifier, as experimentally demonstrated in [28].
- The coefficients are organised in a sparse rotation matrix R_i of dimensionality $n \times \sum_j M_j$ as follows:

$$R_i = \begin{bmatrix} a_{i,1}^{(1)}, ..., a_{i,1}^{(M_1)} & 0 & \cdots & 0 \\ 0 & a_{i,2}^{(1)}, ..., a_{i,2}^{(M_2)} & \cdots & 0 \\ \vdots & \vdots & \ddots & \vdots \\ 0 & 0 & \cdots & a_{i,K}^{(1)}, ..., a_{i,K}^{(M_K)} \end{bmatrix}$$

The columns of R_i are rearranged to R_i^a with respect to the original feature set to construct the training set XR_i^a for the classifier D_i.

3.2.2. Classification

For a given test sample $\mathbf{x}$, let $d_{i,j}(xR_i^a)$ be the probability assigned by the classifier D_i that x belongs to class w_j. The confidence for each class, i.e., w_j, is calculated by the average combination method as

$$\mu_j(\mathbf{x}) = \frac{\mathbf{1}}{\mathbf{L}} \sum_{\mathbf{i=1}}^{\mathbf{L}} \mathbf{d_{i,j}}(\mathbf{xR_i^a}), \mathbf{j} = \mathbf{1}, ..., \mathbf{c}, \tag{7}$$

where L is the ensemble size. $\mathbf{x}$ is assigned to the class with the largest confidence. The percentage of correct classification rate is CCR = $s_c/s_t * 100$, where s_c and s_t are respectively the number of correctly identified subjects and the total number of subjects in the dataset. To increase the statistical significance of the results, CCR is obtained as the average of 10 runs for specified values of L and the number of features, M. The CCR at rank-r implies that the correctly identified subjects are among the top r confidence

values with their matching gallery classes. Thus, CCR at rank-1 implies that the probe subjects result in the highest confidence values with their matching gallery classes, similarly CCR at rank-5 implies that the correctly identified probe subjects are within the top 5 highest confidence values.

3.2.3. Sensitivity of Parameters

The key parameters of rotation forest are L and M. Since the aim of the paper is to demonstrate the efficacy of the application of Gaussian filtering at multiple cut-off frequencies to achieve robustness to unpredictable variation in clothing and carrying conditions rather than achieve higher W-AvgI through intensive parameter calibration, we fix M=5 for all values of L used in the proposed method, as very high value of M causes overlearning.

4. Experiments

The proposed method is evaluated using two public datasets: USF HumanID gait challenge dataset [22] and OU-ISIR treadmill gait dataset B [18].

The HumanID gait challenge problem in [22] has three aspects: a dataset, 12 challenge experiments and a baseline algorithm. The large version of USF HumanID gait challenge dataset comprises 1870 sequences of 122 subjects walking along an elliptical path in an outdoor environment in front of two cameras. The dataset provides up to 32 possible testing conditions by combining the following five covariates: (a) walking surface (grass (G) or concrete (C)); (b) shoe type (A or B); (c) viewpoint (right (R) or left (L)); (d) carrying conditions (carrying a briefcase (BF) or not carrying a briefcase (NB)); and (e) elapsed time between the acquisition of the sequences (May (M) or November (N)). The 12 challenge experiments, i.e., probe sets (A to L), are designed for investigating the effects of five covariates on gait recognition. The structure of the probe sets as standardized in [22] is shown in Table 1. All probe sets do not contain the same number of subjects, and there are no common gait sequences between the gallery set and any of the probe sets.

The dataset provides centre-aligned and scale-normalised silhouettes of fixed size 128×88 which could be downloaded from http://figment.csee.usf.edu/GaitBaseline/. As explained in the baseline algorithm, the silhouette bounding boxes of the first, last and the middle frames of a gait sequence are computed manually, and the bounding boxes of the intermediate frames are generated using linear interpolation. After the semi-automated process of bounding box estimation, the iterative expectation-maximisation process of background subtraction is used to extract the foreground, i.e., the silhouette. The silhouette is normalised to a height of 128 pixels, and centralised by coinciding its centre-of-mass with the centre of the frame.

Table 1 shows the classification rates of the proposed method using L = 10, 50 at ranks 1 and 5 for comparison with the state-of-the-art methods that outperform Baseline on the USF dataset. All methods in Table 1 use the same gallery set (G, A, R, NB, M/N) to report the identification rates for the 12 challenge experiments as specified by the USF dataset (see the first three rows of

Table 1. Classification rates (%) at rank-1 and rank-5 of the gait recognition methods on full version of USF HumanID gait challenge dataset using the gallery set (G, A, R, NB, M/N) of 122 subjects. Keys for covariates: V - view; H - shoe; S - surface; B - briefcase; T - time; and C - clothes.

Probe Set	A	B	C	D	E	F	G	H	I	J	K	L	W-AvgI
Probe Size	122	54	54	121	60	121	60	120	60	120	33	33	-
Covariate	V	H	VH	S	SH	SV	SHV	B	BH	BV	THC	STHC	-
Rank-1 Identification Rate													
GEI [11]	90	91	81	56	64	25	36	64	60	60	6	15	57.66
GTDA-GF [24]	91	93	86	32	47	21	32	95	90	68	16	19	60.58
CGI [26]	91	93	78	51	53	35	38	84	78	64	3	9	61.69
DNGR [16]	85	89	72	57	66	46	41	83	79	52	15	24	62.81
STS-DM [4]	93	96	86	70	69	39	37	78	71	66	27	22	66.68
GPDF-NN [29]	90	91	85	53	52	32	28	92	86	64	12	15	62.99
GPDF-LGSR [29]	95	93	89	62	62	39	38	94	91	78	21	21	70.07
VI-MGR [5]	95	96	86	54	57	34	36	91	90	78	31	28	68.13
Proposed method (L=10)	96	96	89	60	62	35	36	93	92	78	33	29	70.10
Proposed method(L=50)	96	96	90	62	63	37	39	94	93	80	41	32	71.74
Rank-5 Identification Rate													
GEI [11]	94	94	93	78	81	56	53	90	83	82	27	21	76.23
GTDA-GF [24]	98	99	97	68	68	50	56	95	99	84	40	40	77.58
CGI [26]	97	96	94	77	77	56	58	98	97	86	27	24	79.12
DNGR [16]	96	94	89	85	81	68	69	96	95	79	46	39	82.05
STS-DM [4]	97	98	96	82	83	61	60	95	89	83	39	28	80.48
GPDF-NN [29]	98	94	94	82	79	57	53	99	98	88	33	36	80.84
GPDF-LGSR [29]	99	94	96	89	91	64	64	99	98	92	39	45	85.31
VI-MGR [5]	100	98	96	80	79	66	65	97	95	89	50	48	83.75
Proposed method (L=10)	100	98	96	84	81	66	65	97	95	89	54	52	84.66
Proposed method(L=50)	100	98	97	88	85	68	68	98	95	91	57	54	86.46

Table 1). Since there are different number of probe subjects in the challenge experiments, the weighted average classification rate (W-AvgI) is obtained using [4, 29]

$$\text{W-AvgI} = \frac{\sum_{i=1}^{g} w_i x_i}{\sum_{i=1}^{g} w_i}, \tag{8}$$

where g denotes the number of challenge experiments, i.e., 12, for Exp. A-L, x_i denotes the CCR of the ith challenge experiment and w_i denotes the number of probe subjects participating in that experiment. Table 1 shows the final W-AvgI of VI-MGR computed by averaging the identification rates obtained by weighted random subspace learning for eighty randomly chosen values of number of subspaces in the range [100,500]. The table shows that our method achieves W-AvgI) =71.74% at rank-1 and 86.46% at rank-5 for L=50, thus outperforming all other methods. The performance of our method is analyzed using cumulative match characteristic (CMC) curve for the 12 challenge experiments (see Fig. 6(a)). According to this curve, W-AvgI at rank r implies that the percentage of correctly identified subjects is among the top r largest confidence values.

4.1. OU-ISIR Treadmill Gait Dataset

The OU-ISIR gait dataset [18] consists of four components, i.e., dataset A, dataset B, dataset C and dataset D to respectively facilitate the evaluation of gait recognition methods in the presence of variations in speed, clothing, view, and gait fluctuation. Our method is evaluated on the dataset B which comprises 68 subjects with up to 32 combinations of different types of clothing. Table 2 shows these clothing combinations based on the 15 different types of clothes used in constructing the dataset [13]. The dataset defines the combination of regular pant and full shirt as the standard clothing type (type 9). The dataset is divided into (a) a training

Table 2. Different clothing combinations used in the OU-ISIR B dataset. Keys for different types of clothes: RP-Regular pants; BP-Baggy pants; SP-Short pants; Sk-Skirt; CP: Casual pants; HS-Half shirt; FS- Full shirt; LC-Long coat; Pk-Parker; DJ-Down jacket; CW-Casual wear; RC-Rain coat; Ht-Hat; Cs-Casquette cap; Mf-Muffler.

Type	S_1	S_2	S_3	Type	S_1	S_2	Type	S_1	S_2
3	RP	HS	Ht	0	CP	CW	F	CP	FS
4	RP	HS	Cs	2	RP	HS	G	CP	Pk
6	RP	LC	Mf	5	RP	LC	H	CP	DJ
7	RP	LC	Ht	9	RP	FS	I	BP	HS
8	RP	LC	Cs	A	RP	Pk	J	BP	LC
C	RP	DJ	Mf	B	RP	Dj	K	BP	FS
X	RP	FS	Ht	D	CP	HS	L	BP	Pk
Y	RP	FS	Cs	E	CP	LC	M	BP	DJ
N	SP	HS	-	P	SP	Pk	R	RC	-
S	Sk	HS	-	T	Sk	FS	U	Sk	PK
V	Sk	DJ	-	Z	SP	FS	-	-	-

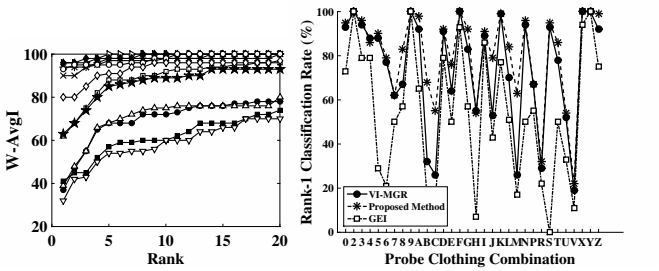

(a) (b)

Fig. 6. (a) Performance analysis using CMC curve on 12 challenge experiments of USF gait data set. Keys: '▷'- Exp. A (Probe: G, A, L, NB, M/N); '◇'- Exp. B (Probe: G, B, R, NB, M/N); '×'- Exp. C (Probe: G, B, L, NB, M/N); '□'- Exp. D (Probe: C, A, R, NB, M/N); '⋆'- Exp. E (Probe: C, B, R, NB, M/N); '•'- Exp. F (Probe: C, A, L, NB, M/N); '△'- Exp. G (Probe: C, B, L, NB, M/N); '∗'- Exp. H (Probe: G, A, R, BF, M/N); '○'- Exp. I (Probe: G, B, R, BF, M/N); '◆'- Exp. J (Probe: G, A, L, BF, M/N); '■'- Exp. K (Probe: G, A/B, R, NB, N); and '▽'- Exp. L (Probe: C, A/B, R, NB, N); (b) Rank 1 classification rate for 32 probe items of OU-ISIR dataset B with different clothing combinations using gallery set of subjects with RP+FS.

set comprising 446 sequences of 20 subjects with all types of clothes; (b) a gallery set comprising sequences of the remaining 48 subjects with standard clothes (type 9); and (c) a probe set comprising 856 sequences for these 48 subjects with other types of clothes excluding the standard clothes.

Unlike the method in [13], the goal of our method is to demonstrate robustness against unpredictable variation in clothing. Hence, unlike [13], we do not use the training dataset to train our system with all possible types of clothing combinations. We evaluated GEI on OU-ISIR dataset B using gallery and probe sets each comprising 48 subjects to compare with the proposed method. Fig. 6(b) shows the results of comparisons with GEI and VI-MGR (available from [5]). The figure shows that our method significantly outperforms GEI and VI-MGR at rank-1 CCR.

5. Conclusion and future work

The paper introduces a gait representation, AGKI, by averaging each of the five key frames of a gait period over a gait sequence. The AGKIs are subjected to Lp-Gf and Hp-Gf at different cut-off frequencies to achieve invariance to unpredictable variation in clothing and carrying conditions. The paper also introduces the application of rotation forest ensemble classifier in gait recognition.

Experimental analyses on two public datasets demonstrate the efficacy of the method.

Future studies will include: (a) taking into consideration of view-invariant gait characteristics while forming AGKI to achieve robustness to variation in view by developing a view transformation model; (b) detailed experimental analyses on the choice of L and M to achieve improved identification rate.

References

[1] Bashir, K., Xiang, T., Gong, S., 2010. Gait recognition without subject cooperation. Pattern Recognition Letters 31, 2052–2060.
[2] Breiman, L., 1996. Bagging predictors. Machine Learning 24, 123–140.
[3] Choudhury, S.D., Tjahjadi, T., 2012. Silhouette-based gait recognition using procrustes shape analysis and elliptic fourier descriptors. Pattern Recognition 45, 3414–3426.
[4] Choudhury, S.D., Tjahjadi, T., 2013. Gait recognition based on shape and motion analysis of silhouette contours. Computer Vision and Image Understanding 117, 1770–1785.
[5] Choudhury, S.D., Tjahjadi, T., 2015. Robust view-invariant multiscale gait recognition. Pattern Recognition 48, 798–811.
[6] Freund, Y., Schapire, R., 1997. A decision-theoretic generalization of on-line learning and an application to boosting. Journal of Computer and System Sciences 55, 119–139.
[7] G. Bradski, A.K., 2008. Learning OpenCV Computer Vision with the OpenCV Library. 1st ed., O'Reilly Media, Sebastopol.
[8] Gonzalez, R.C., Woods, R.E., 1992. Digital image processing. 2nd ed., Addison-Wesley, USA.
[9] Gu, J., Ding, X., Wang, S., Wu, Y., 2010. Action and gait recognition from recovered 3-d human joints. IEEE Transactions on Systems, Man and Cybernetics, Part B: Cybernetics 40, 1021–1033.
[10] Guan, Y., Li, C.T., Hu, Y., 2012. Random subspace method for gait recognition. in: Proceedings of the IEEE International Conference on Multimedia and Expo Workshop (ICMEW'12) , 9–13.
[11] Han, J., Bhanu, B., 2006. Individual recognition using gait energy image. IEEE Transactions on Pattern Analysis and Machine Intelligence 28, 316–322.
[12] Ho, T.K., 1998. The random subspace method for constructing decision forests. IEEE Transactions on Pattern Analysis and Machine Intelligence 20, 832–844.
[13] Hossain, M.A., Makihara, Y., Wang, J., Yagi, Y., 2010. Clothing-invariant gait identification using part-based clothing categorization and adaptive weight control. Pattern Recognition 43, 2281–2291.
[14] Ioannidis, D., Tzovaras, D., Damousis, I.G., Argyropoulos, S., Moustakas, K., 2007. Gait recognition using compact feature extraction transforms and depth information. IEEE Transactions on Information Forensics and Security 2, 623–630.
[15] Lam, T.H.W., Cheung, K.H., Liu, J.N.K., 2011. Gait flow image: A silhouette-based gait representation for human identification. Pattern Recognition 44, 973–987.
[16] Liu, Z., Sarkar, S., 2006. Improved gait recognition by gait dynamics normalization. IEEE Transactions on Pattern Analysis and Machine Intelligence 28, 863–876.
[17] Lu, H., Plataniotis, K.N., Venetsanopoulos, A.N., 2008. A full-body layered deformable model for automatic model-based gait recognition. EURASIP Journal on Advances in Signal Processing , 1–13.
[18] Makihara, Y., Mannami, H., Tsuji, A., Hossain, M.A., Sugiura, K., Mori, A., Yagi, Y., 2012. The ou-isir gait database comprising the treadmill dataset. IPSJ Transactions on Computer Vision and Applications, Technical Note 4, 53–62.
[19] Nayar, S.K., Nakagawa, Y., 1994. Shape from focus. IEEE Transactions on Pattern Analysis and Machine Intelligence 16, 824–831.
[20] Ran, Y., Zheng, Q., Chellappa, R., Strat, T.M., 2010. Applications of a simple characterization of human gait in surveillance. IEEE Transactions on Systems, Man, and Cybernetics, Part B: Cybernetics 40, 1009–1019.
[21] Rodrguez, J.J., Kuncheva, L.I., Alonso, C.J., 2006. Rotation forest: A new classifier ensemble method. IEEE Transactions on Pattern Analysis and Machine Intelligence 28, 1619–1630.
[22] Sarkar, S., Philips, P.J., Liu, Z., Vega, I., Grother, P., Bowyer, K., 2006. The humanid gait challenge problem: data sets, performance, and analysis. IEEE Transactions on Pattern Analysis and Machine Intelligence 27, 162–177.
[23] Tafazzoli, F., Safabakhsh, R., 2010. Model-based human gait recognition using leg and arm movements. Engineering Applications of Artificial Intelligence 23, 1237–1246.
[24] Tao, D., Li, X., Wu, X., Maybank, S.J., 2007. General tensor discriminant analysis and gabor features for gait recognition. IEEE Transactions on Pattern Analysis and Machine Intelligence 29, 1700–1715.
[25] Tenenbaum, J.M., 1970. Accommodation in computer vision. Ph.D. Thesis , Stanford University.
[26] Wang, C., Zhang, J., Wang, L., Pu, J., Yuan, X., 2012. Human identification using temporal information preserving gait template. IEEE Transactions on Pattern Analysis and Machine Intelligence 34, 2164–2176.
[27] Wang, L., Tan, T., Ning, H., Hu, W., 2003. Silhouette analysis-based gait recognition for human identification. IEEE Transactions on Pattern Analysis and Machine Intelligence 25, 1505–1518.
[28] Xia, J., Du, P., He, X., Chanussot, J., 2014. Hyperspectral remote sensing image classification based on rotation forest. IEEE Geoscience and Remote Sensing letters 11, 239–243.
[29] Xu, D., Huang, Y., Zeng, Z., Xu, X., 2012. Human gait recognition using patch distribution feature and locality-constrained group sparse representation. IEEE Transactions on Image Processing 21, 316–326.
[30] Yang, G., Nelson, B., 2000. Wavelet-based autofocusing and unsupervised segmentation of microscopic images. Journal of Science Communication 163, 51–59.